EFFECT OF WORMHOLE DEFECTS ON ELECTRIC FIELD DISTRIBUTION UNDER COMPOSITE VOLTAGE

Emre TUNÇ[1], Murat FİDAN[1]*

[1]*Bolu Abant Izzet Baysal University, Faculty of Engineering, Department of Electrical and Electronics Engineering, 14030, Bolu, Türkiye*

Abstract: The reliability of electrical insulation systems is critical to the continuity of energy transmission and distribution systems. Structural defects that occur in polymer-based insulating materials can affect the distribution of electric fields, leading to partial discharges and subsequently serious failures such as breakdowns. In this study, the effects of wormhole structures with different diameters in cross-linked polyethylene (XLPE) insulators on electric field distribution under alternating current (AC), direct current (DC), and composite voltage (AC+DC) components were numerically investigated using COMSOL Multiphysics software. In the system modeled under a needle-plane electrode configuration, significant increases in both volumetric and surface electric field intensities were observed as the diameter of the wormhole increased. Among all cases, composite voltage conditions resulted in the highest field concentrations, indicating increased electrical stress on the insulation. Additionally, higher field intensities were observed under negative polarity than under positive polarity in all cases. The findings highlight the importance of considering wormhole-type defects in the design of insulating systems and analyzing the electrical stress caused by composite voltage conditions.

Keywords: Wormhole, Composite voltages, Electric field, High voltage

1. Introduction

Today's advancing technology and increasing energy needs make it essential for electrical energy systems to operate more efficiently, reliably, and sustainably (Kadim et al., 2021). In this context, the quality of the insulation systems used is as important as the mechanical and electrical integrity of the production, transmission, and distribution systems. Electrical insulators play a crucial role in preventing failures in transmission and distribution equipment, directly affecting the continuity, safety, and economic operation of energy systems (Ispirli et al., 2022a; Freitas-Gutierres et al., 2024). Deterioration in the performance of insulators can result in serious consequences, such as short circuits, arc formation, or complete failure of equipment functionality (Kavanagh et al., 2020; Tunç and Fidan, 2023; Park et al., 2024). This may impair the integrity of the energy system and pose risks to both system components and connected devices.

Insulation systems operate under increasingly complex electrical stresses in modern systems, where more compact designs are being adopted and higher voltage levels are preferred (Adhikari and Ghassemi, 2024). Insulators operating under high voltage must withstand not only normal operating conditions but also high-frequency pulses (Borghei and Ghassemi, 2022), harmonic voltages (Fidan and Ismailoglu, 2017), composite voltages (Li et al., 2019), transient states

(Annadi and Patsa, 2020), and environmental effects such as temperature and humidity (Roggendorf and Schnettler, 2012; Negari and Moghadam, 2024). Under these conditions, the electrical endurance limits of insulators can be significantly reduced, particularly due to defects in their internal structures or surfaces. Therefore, characterizing defects in insulation systems and quantitatively determining their effects on electric field distribution is crucial for enhancing system reliability and reducing the risk of failure.

Air gaps are among the defects frequently observed in insulating materials (Qiu et al., 2015). Microcracks are also frequently reported in the literature (Dissado and Fothergill, 1992; Stone et al., 2014; Kavanagh et al., 2020). Bubbles and irregular geometric structures can also be considered among other important defects (Tian et al., 2017; Zheng et al., 2021; Zhao et al., 2024). These defects can form during the material's production process or operation and can further intensify the electric field, especially in areas where the electric field is concentrated, such as sharp-tipped electrodes. These field intensifications can lead to the formation of electrical treeing and partial discharge over time (Ghassemi, 2018; Zhang et al., 2021; Adhikari and Ghassemi, 2024). This accelerates the degradation process of the insulating material (Borghei and Ghassemi, 2022; Kavanagh et al., 2020). As a result, permanent damage to the insulation

structure may occur. This can reduce the reliability of power systems and cause serious operational issues.

The wormhole effect (Zhao, 2022), which has been increasingly discussed in the literature in recent years, has been found to be closely related to the formation of partial discharges in insulating materials (Li et al., 2017; Li et al., 2019; Wu et al., 2024). A wormhole is a structural defect in an insulator characterized by the formation of thin, long, channel-like gaps or cracks (Rosenberg et al., 2010; Zhao et al., 2013; Gong et al., 2020). Such structures can cause excessive concentration of the electric field in certain areas, leading to insulation failures such as breakdown, partial discharge, or thermal degradation (Zhao et al., 2013; Li et al., 2017). In this context, the numerical and experimental investigation of the effects of wormhole defects on electric field distribution is of significant importance for enhancing the reliability of insulation systems.

Li et al. (2017) investigated the effect of temperature on partial discharges under DC using an oil-paper insulation model in a configuration with a needle plane electrode. The study also investigated the breakdown characteristics of the insulation material under the wormhole effect. In the study conducted to experimentally verify the wormhole effect (Zhao et al., 2013), bulk breakdown and surface discharge properties were investigated on organic glass and polystyrene samples by applying different pulse durations (10 ns and 7 µs) at different voltage levels (100 kV, 130 kV, and 170 kV). Theoretical evaluations of the fundamental physical mechanisms underlying the wormhole effect were presented by analyzing the surface discharge threshold and delay time. In addition to the wormhole effect, which has been discussed only limitedly in the literature, there are also different studies conducted under non-homogeneous electric fields.

In a study conducted by Lin et al. (2024) the effects of mixed voltage components on the channel discharge formation mechanism were investigated using a 3-electrode configuration consisting of a needle electrode and a pair of parallel plates. Hamidieh and Ghassemi (2024) computationally investigated the effect of different needle electrodes with conical cross-sections on negative corona discharge. The study particularly focuses on Trichel current pulses, which are regular and repetitive small current pulses observed during negative corona discharge. Dordizadeh et al. (2017) presented an experimental study investigating Trichel pulses in a needle-plane electrode geometry. In this study, the effects of parameters such as corona voltage, gap distance, and tip radius on the characteristics of Trichel pulses were investigated.

Saini and Prasad (2024) investigated the surface charging characteristics of polymeric insulators under AC corona discharge at low pressure conditions. Discharge generation was performed under different electrode configurations, including single-needle, double-needle, and triple-needle configurations. Zhao et al. (2017) investigated the discharge characteristics of CF_3I/N_2 gas

mixtures under standard lightning impulse voltage in needle-plane and sphere-plane electrode configurations, which are important for CF_3I and its mixtures used in electrical equipment. Chen et al. investigated the breakdown characteristics of the SF_6/N_2 gas mixture under an extremely non-uniform electric field using an experimental setup isolated from external influences (Chen et al., 2022). In another study, Chen et al. (2019) conducted an experimental study on negative corona discharges under a needle-plane electrode configuration in a container where gas humidity and pressure could be precisely controlled. In this study, the transition characteristics of discharge modes were examined in detail under the influence of electrode curvature radius, humidity, and pressure.

The behavior of wormhole-type structural internal defects in insulating materials under complex stresses remains an area that has yet to be explored in the literature. This study aims to numerically investigate the effects of wormhole structures with different diameters on the electric field distribution under composite voltage conditions consisting of AC and DC components. Simulation analyses performed in the COMSOL Multiphysics environment were used to evaluate how volumetric and surface electric field intensities vary depending on the presence and size of structural defects in the material. The obtained results are expected to contribute to the existing knowledge on the behavior of insulation systems and provide a foundation for future experimental or theoretical studies.

2. Materials and Methods

2.1. Composite Voltages

Electrical insulation systems are often subjected not only to a single type of voltage stress but to the simultaneous influence of multiple voltage components (Ispirli et al., 2022a). In the literature, insulation systems have been investigated under AC conditions (Hu et al., 2022; Yang et al., 2022). Similarly, there are investigations conducted under DC (Beroual et al., 2013; Muppala and Reddy, 2021). Moreover, in some studies, insulation systems have been evaluated solely under the influence of impulse voltage. (Liang et al., 2020; Reddy et al., 2023). However, in real operating conditions, especially in modern power systems, these voltage components may occur together. The AC + DC composite voltage resulting from the simultaneous application of AC and DC components can cause stress beyond standard test conditions, significantly affecting the voltage withstand capability of insulation systems. In this case, the resulting electric field distribution differs from that formed under AC or DC alone, which may cause regional field concentrations and early insulation degradation.

The widespread adoption of HVDC technologies has increased the need for AC–DC conversion in power transmission and has led to the widespread use of power electronics-based systems. In parallel with these developments, it has become more likely for electrical

equipment to operate under composite voltages, including both AC and DC components. Therefore, tests conducted under single voltages alone may be insufficient to represent the actual operating conditions of the systems. In particular, when the positive or negative component of the DC voltage combines with the AC voltage, the electrical discharge mechanism and breakdown voltage behavior can vary significantly depending on the polarity (Ispirli et al., 2022b).

In this context, examining the effects of composite voltages on insulation systems is important not only from a theoretical perspective but also in terms of understanding performance under real-world conditions. In particular, a detailed assessment of insulation behavior under composite voltages consisting of AC and DC components plays a critical role in the design and validation processes of new-generation power systems.

2.2 Geometrical and Electrical Configuration of the Test System

This section presents a simulation study of wormhole structures modeled in insulating material under a non-uniform electric field at different voltage levels and types. The needle-plane electrode configuration was modeled using the COMSOL Multiphysics program. In the study, the electric field distribution in the insulation system was analyzed in detail using COMSOL Multiphysics software for different wormhole diameters. The Electric Currents module was used for the electric field distribution analysis.

The structural features and electrical parameters of the system modeled in the COMSOL Multiphysics environment are presented in Table 1.

A stainless steel disc with a thickness of 5 mm and a diameter of 300 mm was modeled as the plane electrode. The diameter of the plane electrode was determined based on similar studies in the literature (Lan et al., 2012).

Stainless steel was selected as the electrode material due to its high electrical conductivity, corrosion resistance, and experimental repeatability, which is also a preferred approach in (Timoshkin et al., 2009).

The needle electrode was modeled with a curvature radius of 100 μm and a length of 50 mm using stainless steel material due to these advantages. The material and dimensional specifications of the needle electrode were determined based on similar studies in the literature (Liu et al., 2013; Rubinetti et al., 2024). In the COMSOL Multiphysics environment, the gap between the electrodes was set to 2 mm. XLPE is widely used as a cable insulation material due to its excellent insulation performance, favorable electrical and mechanical properties, and cost-effectiveness (Dong et al., 2019). Therefore, XLPE with dimensions of 2 × 400 × 400 mm (thickness × width × length) was selected as the insulating material in this study. Wormhole channels with various diameters were introduced within the volume of the insulating material. The entire test model was constructed using COMSOL's built-in CAD tools, and tetrahedral mesh elements with a maximum size of 5 mm were used. Visual representations of the model's geometric dimensions are presented in Figure 1.

The electric field distribution of the insulator and electrode configuration modeled in the COMSOL Multiphysics environment was analyzed under different voltage levels and types. The voltage waveforms used in the study were generated by the IEC 60060-1:2010 standard. This standard defines the technical principles for high-voltage testing under composite voltage conditions (Dedeoglu and Merev, 2023; IEC 60060-1:2010 - High-Voltage Test Techniques - Part 1: General Definitions and Test Requirements, 2010). These voltage levels and types are listed in Table 2.

**Table 1.** Structural features of the modeled test system

Parameter	Description / Value
Electrode Configuration	Needle–Plane Electrode (Stainless Steel Material)
Needle Electrode Size	r_{tip}= 100 μm, h= 50 mm
Plane Electrode Size	r=300 mm, thickness= 5 mm
Insulating MaterialSize and Type	2 x 400 x 400 mm (thickness × width × length) XLPE ($\varepsilon_{XLPE} = 2.4$)
Wormhole Channel Diameter	0 μm ,50 μm, 75 μm, 100 μm, 150 μm, 200 μm

Table 2. Voltage types applied to the test model along with associated mathematical expressions

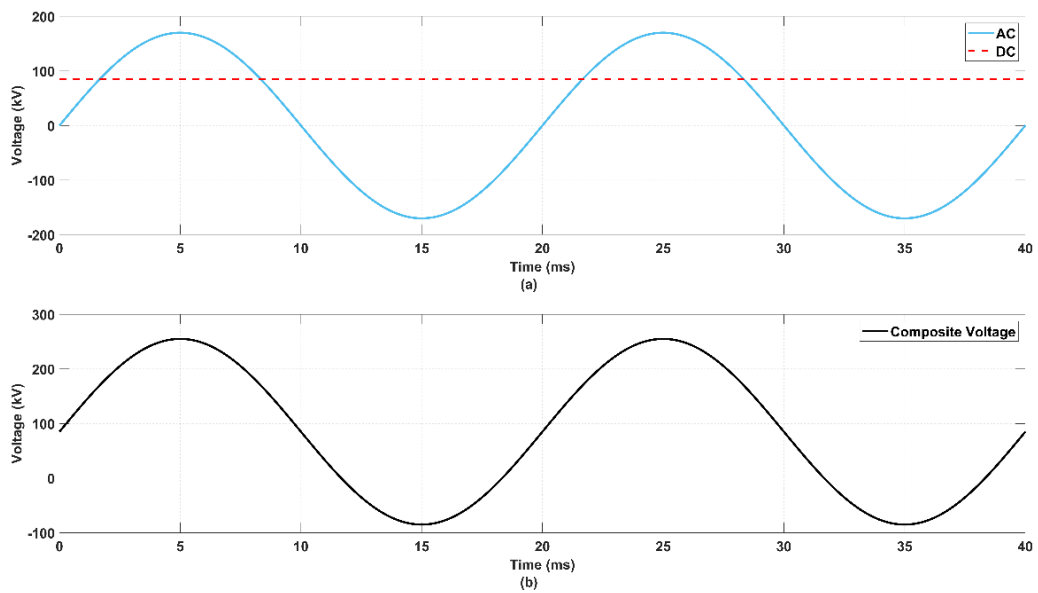| Voltage Type	Mathematical Expression of Voltage
AC	$V_{AC} = 170000\sin(2\pi ft)\ V$
DC	$V_{DC} = 85000\ \text{V}$
Composite Voltage	$V_{composite} = 170000\sin(2\pi ft) + 85000\ V$
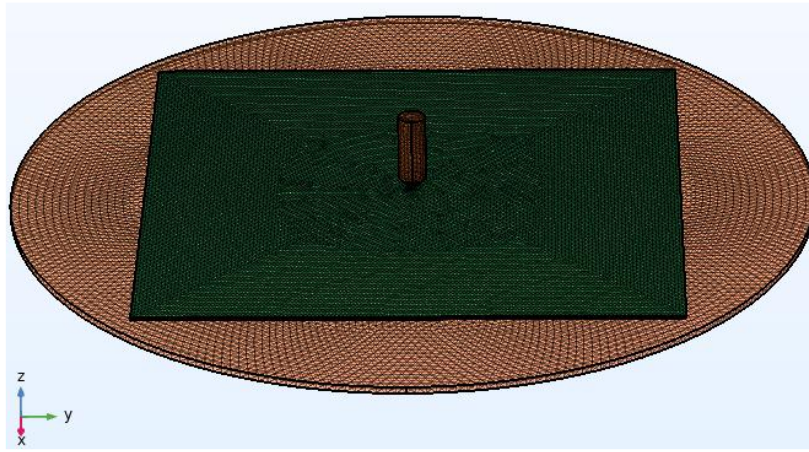
(a)
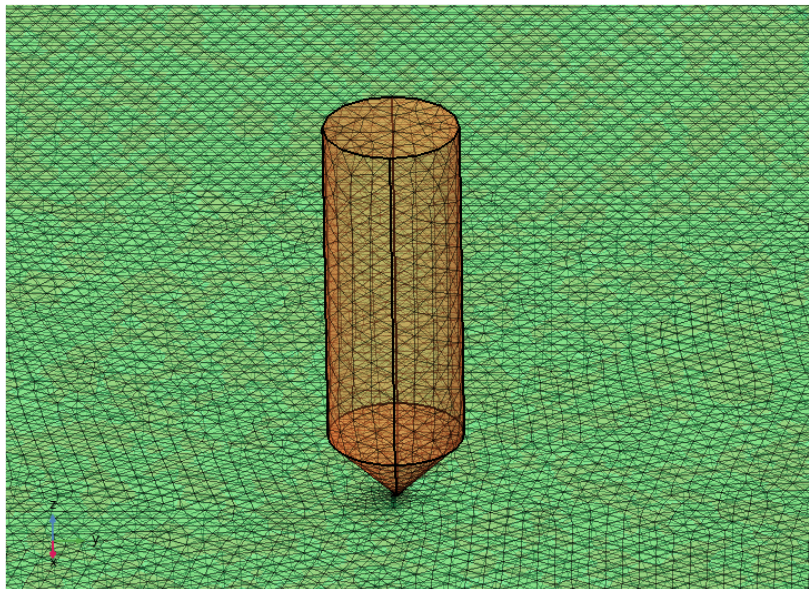
(b)

Figure 1. The designed model: (a) the network architecture, (b) a detailed view of the network architecture.

Figure 2. (a) The AC and DC voltage waveforms generated using MATLAB/Simulink, (b) the composite voltage waveform.

In order to analyze the test model designed in the COMSOL Multiphysics environment under composite voltage conditions, the required voltage waveforms were generated in the MATLAB/Simulink environment and then transferred to COMSOL Multiphysics. The time-dependent variations of the generated AC, DC, and composite voltage signals in MATLAB/Simulink are presented in Figure 2.

Although there is no standardized ratio for the application of AC–DC composite voltages in the literature, various ratios have been investigated in different studies. In this context, some studies have preferred a 1:1 ratio so that the amplitudes of the AC and DC components are equal (Li et al., 2025; Zhou et al., 2020). Additionally, ratios such as 1:3, 1:5, and 1:7 have also been examined to evaluate the effects of different DC levels (Zhou et al., 2020). In other studies, the DC component has been applied at levels corresponding to 1%, 3%, 5%, and 10% of the AC peak value (Ispirli et al., 2021a). Furthermore, a wide range of ratios have been tested using a constant 5 kV AC voltage combined with DC voltages varying from −25 kV to +20 kV (Ispirli et al., 2022b).

This variety indicates that system behavior is sensitive to the AC–DC ratio and that a specific standard has not yet been established. Accordingly, in this study, a 2:1 ratio was adopted, and a composite voltage consisting of a 170 kV peak AC at 50 Hz and an 85 kV DC was simultaneously applied to the electrodes in the COMSOL Multiphysics environment. The 170 kV AC peak value was determined based on the voltage levels commonly preferred in similar studies in the literature (Zhao et al., 2013). This voltage level was selected to enable a clear observation of the effects of AC and DC components on the insulating material, as well as to allow comparisons with different ratios presented in the literature.

In electric power systems, overvoltage-induced failures can vary depending on the amplitude of the operating voltage. In this study, to analyze the most critical conditions in the power system, the electric field distribution was examined based on the peak values of both AC and composite voltages. For this reason, the electric field distribution within the test model was analyzed at two specific time instances: t = 0.005 s (corresponding to the voltage maximum) and t = 0.015 s (corresponding to the voltage minimum). The test model, designed in the COMSOL Multiphysics environment, was evaluated under six different cases: five with varying wormhole channel diameters and one without any wormhole effect. The types of voltage signals applied to the electrodes in these six cases are presented in Table 3.

Table 3. Voltage waveforms applied to the test model for six different cases

Case	Voltage Type	Mathematical Expression of Voltage	Wormhole Diameter
Case 1	AC	$V_{AC}=170000\sin(wt)$	No wormhole
	DC	$V_{DC}=85000$	
	Composite Voltage	$V_{composite}=170000\sin(wt)+85000$	
Case 2	AC	$V_{AC}=170000\sin(wt)$	50 μm
	DC	$V_{DC}=85000$	
	Composite Voltage	$V_{composite}=170000\sin(wt)+85000$	
Case 3	AC	$V_{AC}=170000\sin(wt)$	75 μm
	DC	$V_{DC}=85000$	
	Composite Voltage	$V_{composite}=170000\sin(wt)+85000$	
Case 4	AC	$V_{AC}=170000\sin(wt)$	100 μm
	DC	$V_{DC}=85000$	
	Composite Voltage	$V_{composite}=170000\sin(wt)+85000$	
Case 5	AC	$V_{AC}=170000\sin(wt)$	150 μm
	DC	$V_{DC}=85000$	
	Composite Voltage	$V_{composite}=170000\sin(wt)+85000$	
Case 6	AC	$V_{AC}=170000\sin(wt)$	200 μm
	DC	$V_{DC}=85000$	
	Composite Voltage	$V_{composite}=170000\sin(wt)+85000$	

3. Results and Discussion

3.1 Simulation Results

This section presents the results of electric field analyses under composite voltage components for the test model designed using the COMSOL Multiphysics program. Detailed electric field distribution analyses were performed for six different cases of XLPE material under a needle-plane electrode configuration. For the cases specified in Table 3, the simulation duration in COMSOL Multiphysics was set to 20 ms, with a time resolution of 10^{-4} seconds. The analysis results for Case 1 are presented in Figure 3.

In the simulation studies conducted without the influence of the wormhole effect, a maximum volumetric electric field intensity (E_{maxvol}) of 2282.76 kV/cm was observed

within the volume of the insulating material under AC at t = 0.005 s. At the negative peak value of the AC (at t = 0.015 s), the E_{maxvol} in the insulating material volume was 2288.09 kV/cm. In the first case, which was conducted without the wormhole effect and under DC, the electric field intensity within the insulating material volume reached 1141.38 kV/cm. Under composite voltage, the electric field intensity within the volume of the insulating material was calculated as 3423.08 kV/cm at t = 0.005 s and 1139.90 kV/cm at t = 0.015 s, respectively. On the surface of the XLPE material near the needle electrode, the maximum surface electric field intensities ($E_{maxsurf}$) under AC, DC, and composite voltages at t = 0.005 s were obtained as 45.0348 V/cm (Figure 3.b), 22.5175 V/cm (Figure 3.d), and 67.5316 V/cm (Figure 3.f), respectively.

The results obtained for Case 2 are presented in Figure 4. In the analysis conducted for the wormhole condition with a diameter of 50 μm, the E_{maxvol} within the insulating material under AC voltage was obtained as 14014.2 kV/cm at t = 0.005 s. At t = 0.015 s, corresponding to the negative peak of the AC, the E_{maxvol} was observed to be 14038.1 kV/cm. Under the influence of DC, the E_{maxvol} was obtained as 7024.71 kV/cm. The E_{maxvol} values obtained under composite voltage were 21670.5 kV/cm at t = 0.005 s and 7182.66 kV/cm at t = 0.015 s, respectively. On the surface of the XLPE material near the high-voltage electrode, the $E_{maxsurf}$ at t = 0.005 s under AC, DC, and composite voltages were obtained as 2704.91 V/cm (Figure 4.b), 1763.45 V/cm (Figure 4.d), and 3724.38 V/cm (Figure 4.f), respectively.

The results for Case 3 are presented in Figure 5. For the wormhole structure with a diameter of 75 μm, the E_{maxvol} under AC was obtained as 14926.8 kV/cm at t = 0.005 s. At t = 0.015 s, this value was calculated as 14941.3 kV/cm under the same conditions. Under DC, the E_{maxvol} was found to be 7463.76 kV/cm. In the case of composite voltage, the E_{maxvol} values were determined as 22384.3 kV/cm and 7463.70 kV/cm at t = 0.005 s and t = 0.015 s, respectively. On the surface of the insulating material facing the needle electrode in the test model, the $E_{maxsurf}$ values at t = 0.005 s under AC, DC, and composite voltage were calculated as 2422.42 V/cm (Figure 5.b), 1542.17 V/cm (Figure 5.d), and 3632.66 V/cm (Figure 5.f), respectively.

The results for Case 4 are presented in Figure 6. For the wormhole structure with a diameter of 100 μm, the E_{maxvol} under AC was obtained as 15176.9 kV/cm and 15211.5 kV/cm at t = 0.005 s and t = 0.015 s, respectively. Under DC, the E_{maxvol} was found to be 7891 kV/cm. In the case of composite voltage, the E_{maxvol} was observed to be 22737.2 kV/cm and 7513.01 kV/cm at t = 0.005 s and t = 0.015 s, respectively. For XLPE material, the $E_{maxsurf}$ values under AC, DC, and composite voltage at t = 0.005 s were calculated as 2376.11 V/cm (Figure 6.b), 1302.19 V/cm (Figure 6.d), and 3508.31 V/cm (Figure 6.f), respectively.

The results for Case 5 are presented in Figure 7. For the wormhole structure with a diameter of 150 μm, the E_{maxvol} under AC was observed as 15382.4 kV/cm and 15403 kV/cm at t = 0.005 s and t = 0.015 s, respectively. Under DC, the E_{maxvol} was found to be 8325.27 kV/cm. Under composite voltage, the E_{maxvol} values were obtained as 23068.2 kV/cm and 7691.31 kV/cm at t = 0.005 s and t = 0.015 s, respectively. On the surface of the XLPE material near the high-voltage electrode for Case 5, the $E_{maxsurf}$ values at t = 0.005 s under AC, DC, and composite voltage were calculated as 2257.6 V/cm (Figure 7.b), 1128.89 V/cm (Figure 7.d), and 3385.61 V/cm (Figure 7.f), respectively.

The results for Case 6 are presented in Figure 8. For the wormhole structure with a channel diameter of 200 μm, the E_{maxvol} under AC was obtained as 18375.9 kV/cm and 18400.9 kV/cm at t = 0.005 s and t = 0.015 s, respectively. Under DC, the E_{maxvol} was observed to be 9188.67 kV/cm for the same channel diameter.

(a)

(b)

(c)

(d)

(e)

(f)
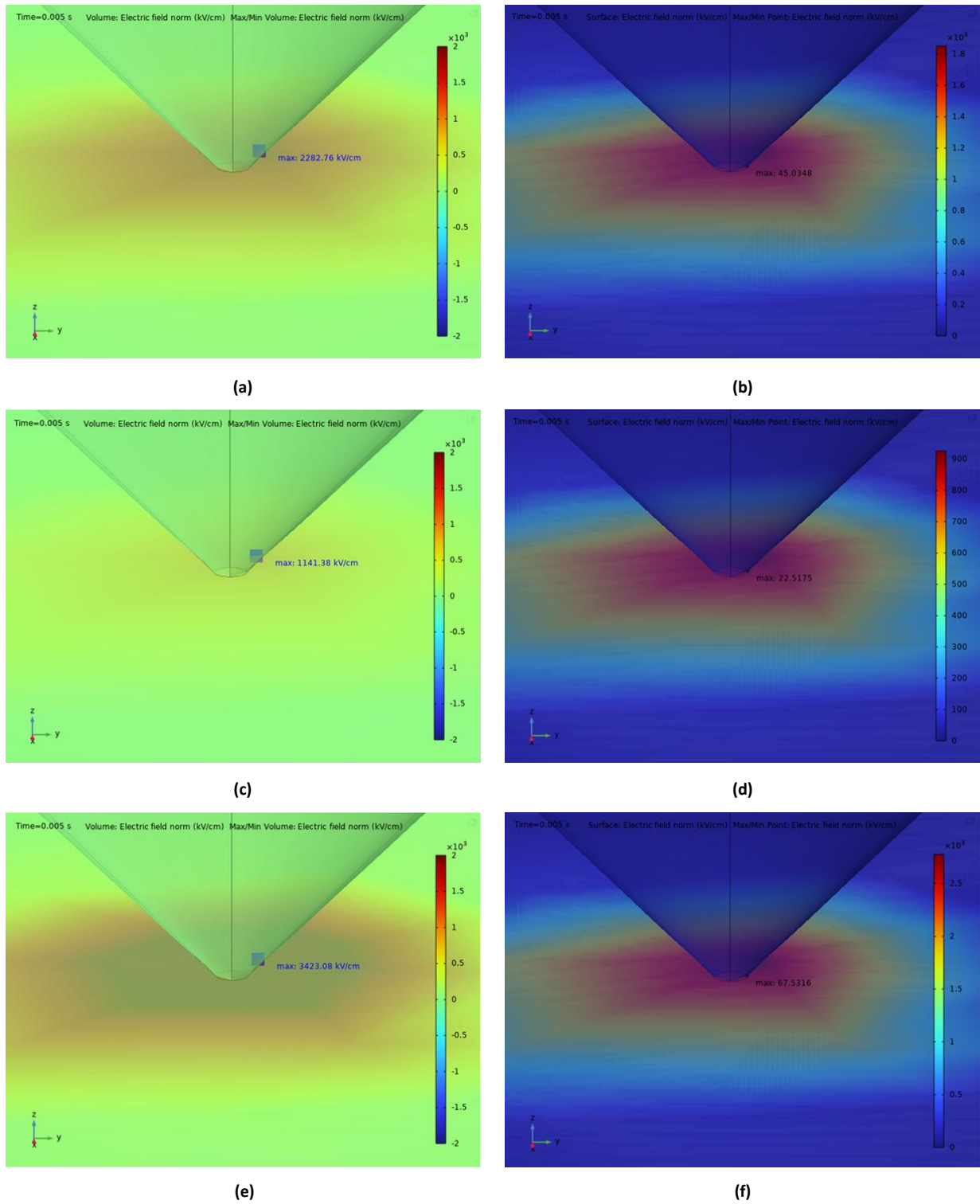
Figure 3. Volumetric (a), (c), (e) and surface (b), (d), (f) electric field distributions obtained for Case 1.

In the test model where a composite voltage was applied, the E_{maxvol} was obtained as 27557.4 kV/cm and 9187.88 kV/cm at t = 0.005 s and t = 0.015 s, respectively. On the surface of the XLPE material near the needle electrode, the $E_{maxsurf}$ values at t = 0.005 s under AC, DC, and composite voltage were calculated as 2145.74 V/cm (Figure 8.b), 1072.96 V/cm (Figure 8.d), and 3217.87 V/cm (Figure 8.f), respectively.

(a)

(b)

(c)

(d)

(e)

(f)
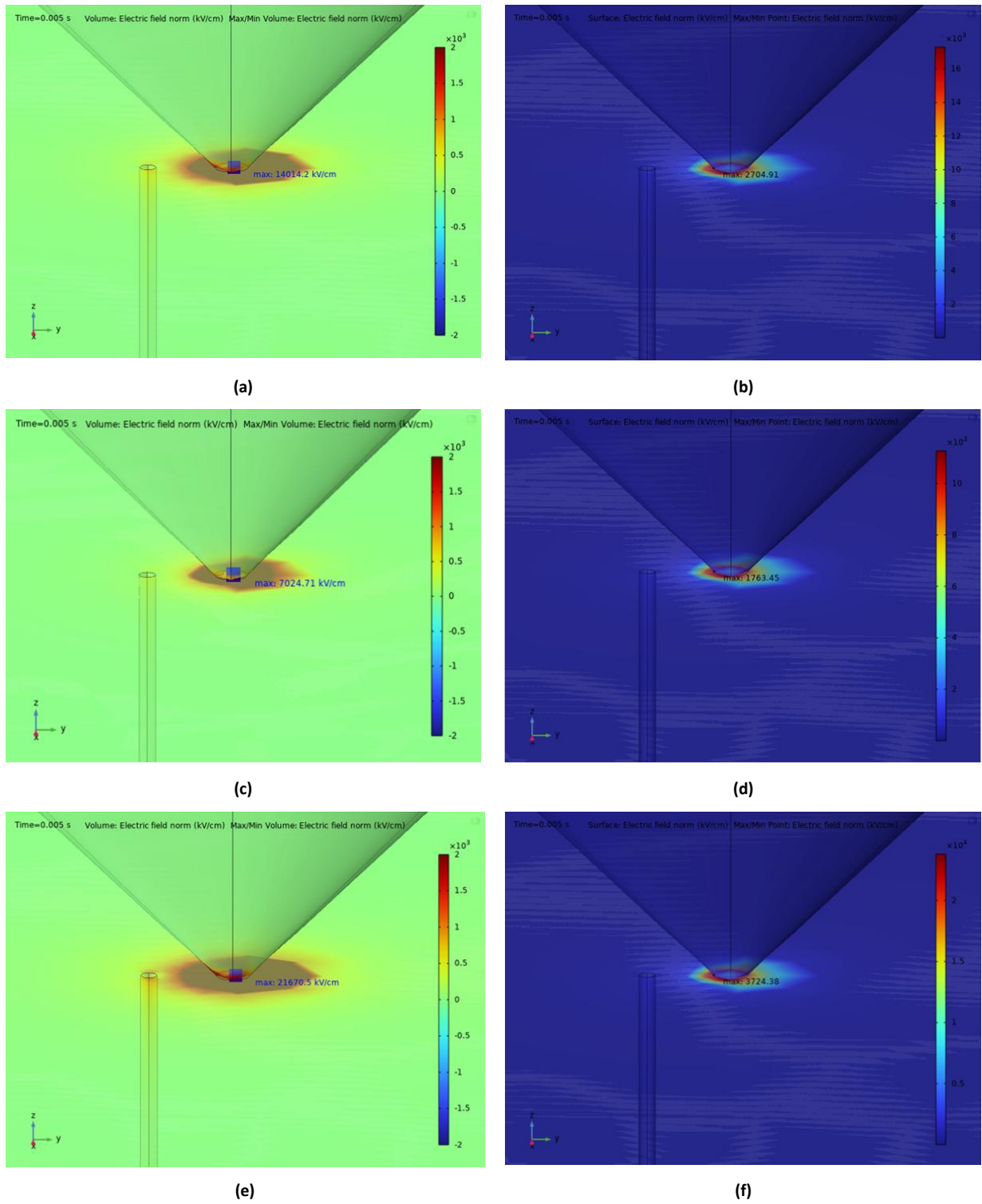
Figure 4. Volumetric (a), (c), (e) and surface (b), (d), (f) electric field distributions obtained for Case 2 (wormhole diameter: 50 µm).
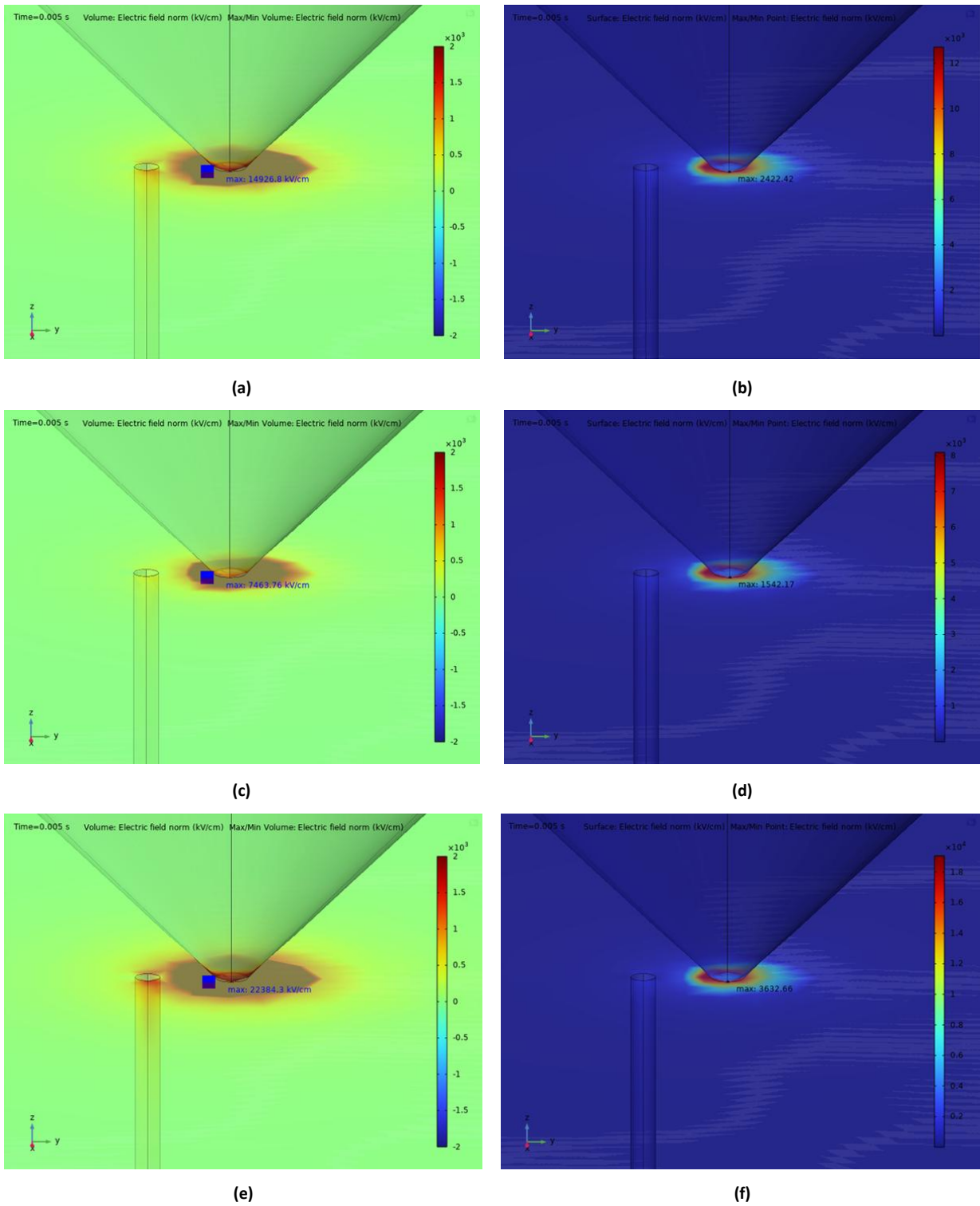
Figure 5. Volumetric (a), (c), (e) and surface (b), (d), (f) electric field distributions for Case 3 (wormhole diameter: 75 µm).

Figure 6. Volumetric (a), (c), (e) and surface (b), (d), (f) electric field distributions obtained for Case 4 (wormhole diameter: 100 µm).

(a)

(b)

(c)

(d)

(e)

(f)

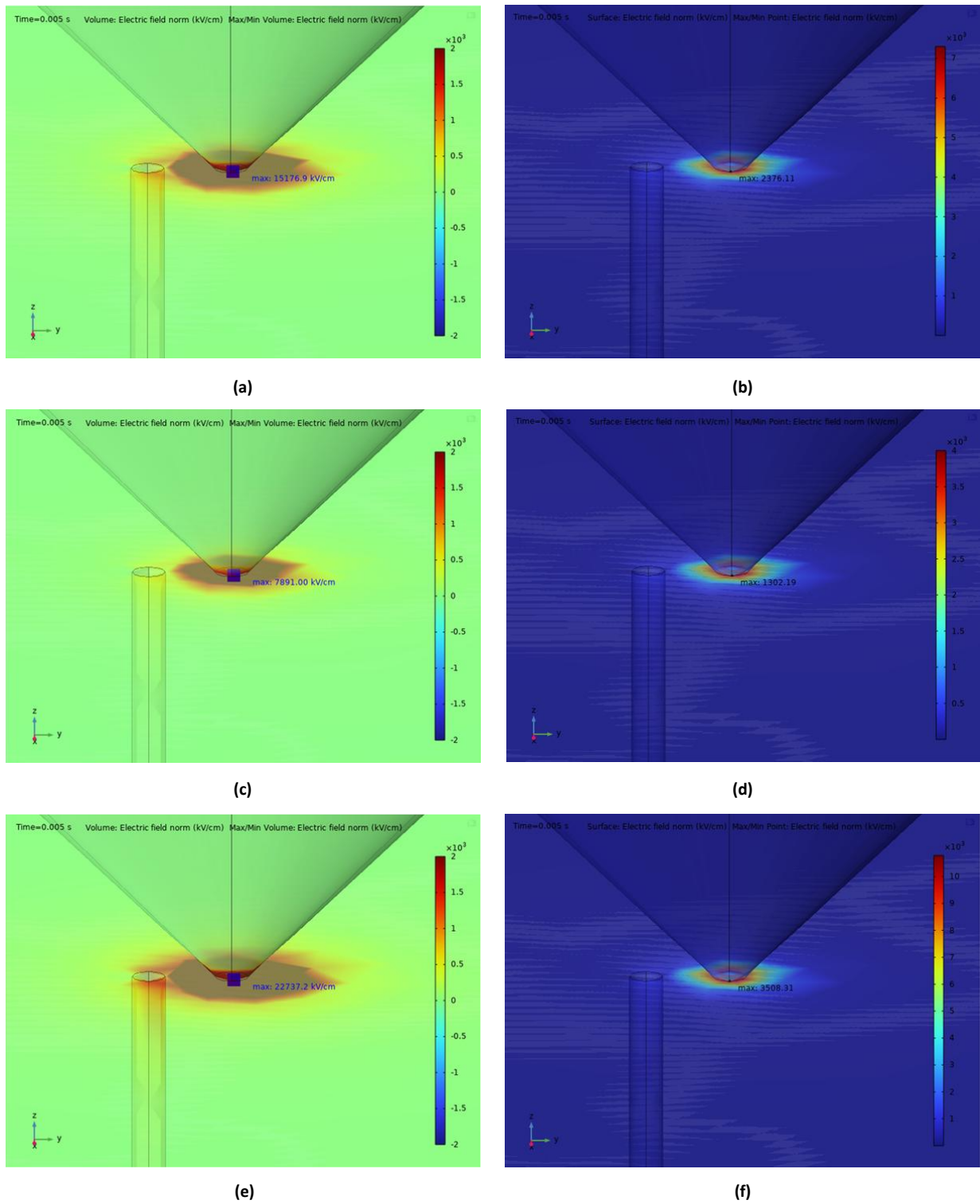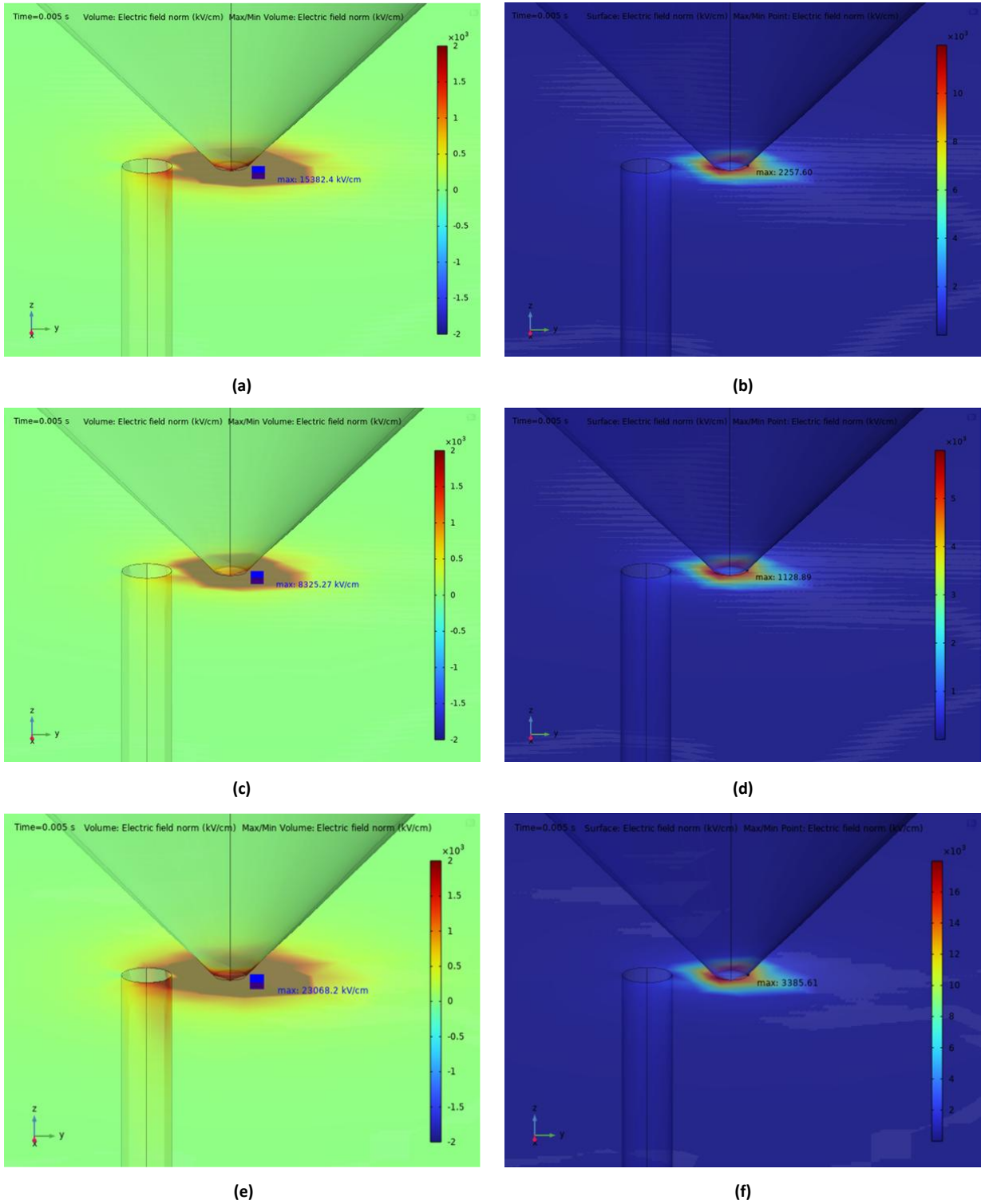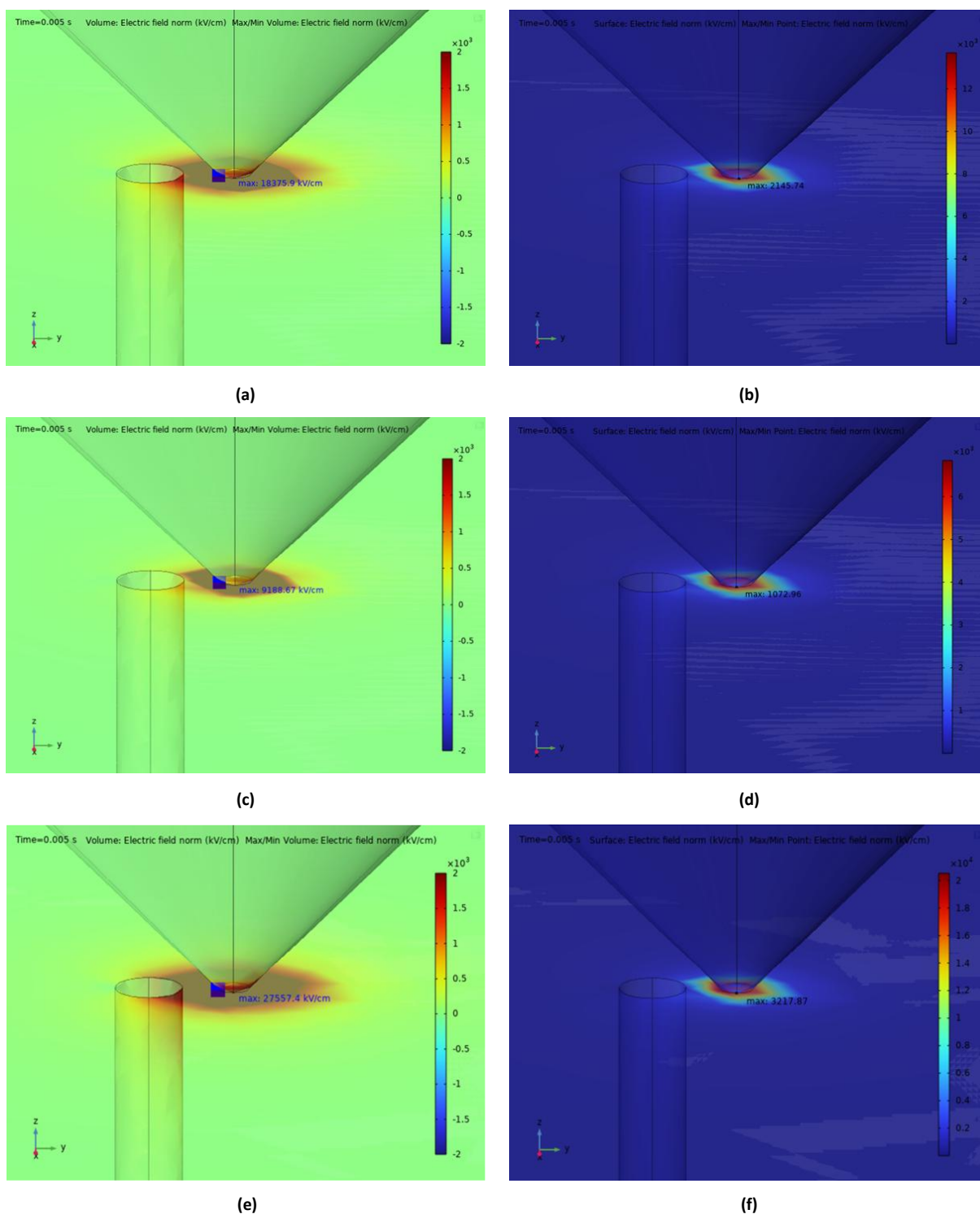**Figure 7.** Volumetric (a), (c), (e) and surface (b), (d), (f) electric field distributions for Case 5 (wormhole diameter: 150 µm).

Figure 8. Volumetric (a), (c), (e) and surface (b), (d), (f) electric field distributions obtained for Case 6 (wormhole diameter: 200 μm).

3.2 Analysis and Comparison of the Results

The test model designed in the COMSOL Multiphysics environment was analyzed under AC, DC, and composite voltage signals. The resulting electric field distributions within the volume and on the surface of the XLPE are presented in Table 4.

The results presented in Table 4 indicate that both the wormhole structures with different diameters and the various voltage types (AC, DC, and composite voltage)

significantly influence the electric field distribution in the XLPE insulating material. In the reference case without any wormhole defects (Case 1), the E_{maxvol} under composite voltage was obtained as 3423.08 kV/cm. In contrast, the $E_{maxsurf}$ remained limited to 67.5316 V/cm. This situation indicates that in an insulating environment without any structural damage, the electric field distribution is more regular and the field concentration is limited.

Table 4. Electric field intensities obtained in the volume and on the surface of the insulating material for six different cases

Case 1 – No Wormhole			
Voltage Type	E_{maxvol} kV/cm		$E_{maxsurf}$ V/cm
	t=0.005 s	t=0.015 s	t=0.005 s
AC	2282.76	2288.09	45.0348
DC	1141.38	1141.38	22.5175
Composite Voltage	3423.08	1139.90	67.5316
Case 2 – Wormhole Diameter = 50 μm			
Voltage Type	E_{maxvol} kV/cm		$E_{maxsurf}$ V/cm
	t=0.005 s	t=0.015 s	t=0.005 s
AC	14014.2	14038.1	2704.91
DC	7024.71	7024.71	1763.45
Composite Voltage	21670.5	7182.66	3724.38
Case 3 – Wormhole Diameter = 75 μm			
Voltage Type	E_{maxvol} kV/cm		$E_{maxsurf}$ V/cm
	t=0.005 s	t=0.015 s	t=0.005 s
AC	14926.8	14941.3	2422.42
DC	7463.76	7463.76	1542.17
Composite Voltage	22384.3	7463.70	3632.66
Case 4 – Wormhole Diameter = 100 μm			
Voltage Type	E_{maxvol} kV/cm		$E_{maxsurf}$ V/cm
	t=0.005 s	t=0.015 s	t=0.005 s
AC	15176.9	15211.5	2376.11
DC	7891.00	7891.00	1302.19
Composite Voltage	22737.2	7513.01	3508.31
Case 5 – Wormhole Diameter = 150 μm			
Voltage Type	E_{maxvol} kV/cm		$E_{maxsurf}$ V/cm
	t=0.005 s	t=0.015 s	t=0.005 s
AC	15382.4	15403	2257.6
DC	8325.27	8325.27	1128.89
Composite Voltage	23068.2	7691.31	3385.61
Case 6 – Wormhole Diameter = 200 μm			
Voltage Type	E_{maxvol} kV/cm		$E_{maxsurf}$ V/cm
	t=0.005 s	t=0.015 s	t=0.005 s
AC	18375.9	18400.9	2145.74
DC	9188.67	9188.67	1072.96
Composite Voltage	27557.4	9187.88	3217.87

However, the inclusion of the wormhole defect in the system resulted in a significant increase in both volumetric and surface electric field values. In this context, for the case with a 50 μm diameter wormhole (Case 2), the E_{maxvol} under composite voltage reached 21670.5 kV/cm, representing an approximately 6.5-fold increase compared to the reference case. Likewise, the $E_{maxsurf}$ increased nearly 55 times, reaching 3724.38 V/cm. These results indicate that even small-scale defects can severely disrupt the electric field distribution. It was also observed that as the wormhole diameter increased, the E_{maxvol} showed a rising trend. For the largest diameter of 200 μm (Case 6), the maximum electric field under composite voltage reached 27557.4 kV/cm, representing the highest value among all simulation scenarios. This increase demonstrates that larger wormhole diameters lead to greater local intensification of the electric field. Similarly, a significant increase in surface electric field strength was observed compared to the reference case. The $E_{maxsurf}$ obtained in this scenario reached 3217.87 V/cm, indicating a considerable degree of field concentration.

The values obtained under AC resulted in higher field strengths in all cases compared to the values obtained under DC. This difference can be explained by the higher peak value of the AC and its time-varying nature, which contribute more significantly to field intensification. Since the DC component does not vary with time, it leads to a more stable field distribution with lower maximum values. Furthermore, it was observed that the E_{maxvol} was higher during the negative half-cycle of the AC waveform than during the positive half-cycle. Especially in negative polarity, since the mobility and acceleration tendency of free electrons are higher, channel formation can begin at lower field strengths in high-field regions.

The increased electric field during the negative half-cycle, combined with the non-uniform field distribution and localized intensifications around wormhole defects, supports the initiation of channel discharges. Under negative polarity, the higher mobility and acceleration of free electrons enable channel formation to begin at lower field strengths in high-field regions. This explains the more significant increase in peak electric field values observed near defects under negative polarity compared to positive polarity. Furthermore, polarity has a notable impact on breakdown voltage in non-uniform electric fields (Özkaya, 2008; Ispirli et al., 2022b; Küchler, 2017) Therefore, polarity should be considered a critical factor influencing field intensification and material stress.

Under composite voltage conditions, the combined effect of DC and AC components results in the highest electric field intensities. This is particularly important for the design of insulation systems in HVDC applications, where such mixed electrical stresses can accelerate insulation degradation by exceeding the material's stress-handling capacity.

4. Conclusion

In this study, the electric field distribution caused by wormhole structures of varying diameters within XLPE insulation under alternating current AC, direct current DC, and composite voltage components was numerically investigated using COMSOL Multiphysics software. Under a needle-plane electrode configuration, field intensifications occurring particularly under non-uniform electric field conditions were analyzed in detail.

The analysis results revealed that wormhole structures significantly increase the local electric field intensity within the insulation. In the reference case without a wormhole (Case 1), the E_{maxvol} under composite voltage was 3423.08 kV/cm. With a 200 μm diameter wormhole, it increased to 27557.4 kV/cm. This represents an almost eightfold increase in electric field intensity. Furthermore, in all cases involving wormhole defects, the surface electric field intensity was observed to reach substantially higher values compared to the reference case.

The results also revealed significant differences in terms of the impact of voltage types on electric field distribution. The maximum electric field values observed under AC were considerably higher than those observed under DC. This can be mainly attributed to the higher amplitude of the AC voltage and its continuous variation over time, which causes higher stress on the insulation. In composite voltage applications, the combined effect of both components resulted in more intense and irregular electric field patterns. In particular, the electric field distribution at t = 0.005 s corresponds to the moment when the voltage level reaches its peak under composite voltage, representing the condition of highest electrical stress.

Due to the effect of the negative half-cycle, higher electric field intensities were recorded in all cases compared to the positive half-cycle. This is attributed to the fact that free electrons accelerate more easily under negative voltage. Under negative polarity, electrons are subjected to a stronger electric field, allowing them to gain higher energy. As a result, electrons may move more effectively in defect regions, potentially initiating the discharge process. This can trigger the channel discharge mechanism earlier in regions where the electric field is concentrated. Consequently, the breakdown voltage threshold of the insulation may decrease, increasing the risk of electrical breakdown.

As the diameter of the wormhole defects increases, not only the magnitude but also the distribution characteristics of the electric field were observed to change. Larger channels caused a sharper field concentration around the defect region, potentially creating critical zones that may facilitate partial discharges or electrical breakdown. This finding highlights the importance of defect control, particularly during the manufacturing processes of insulating materials.

In conclusion, this study provides important findings regarding: (i) the electrical risks induced by wormhole defects depending on their size, (ii) the comparative effects of AC, DC, and composite voltages, and (iii) the influence of polarity on field concentration in non-uniform electric field distributions under high voltage stress. The results obtained contribute to the literature and provide an important perspective on the fundamental parameters that must be considered in terms of the design and reliability of insulation systems.

Author Contributions

The percentages of the authors' contributions are presented below. All authors reviewed and approved the final version of the manuscript.

	E.T.	M.F.
C	50	50
D	50	50
S	0	100
DCP	50	50
DAI	50	50
L	60	40
W	40	60
CR	30	70
SR	50	50
PM	50	50

C=Concept, D= design, S= supervision, DCP= data collection and/or processing, DAI= data analysis and/or interpretation, L= literature search, W= writing, CR= critical review, SR= submission and revision, PM= project management.

Conflict of Interest

The authors declared that there is no conflict of interest.

Ethical Consideration

Ethics committee approval was not required for this study because of there was no study on animals or humans.

References

Adhikari P, Ghassemi M. 2024. Navigating strategies to mitigate insulation issues within high power density (U)WBG power module packages: A comprehensive review emphasizing alternative encapsulation materials. IEEE Transact Industry Applicat, 2024: 1–22. https://doi.org/10.1109/tia.2024.3520096

Annadi RR, Patsa CS. 2020. Estimation of switching surge flashover rate of 1200-kV UHVAC transmission line considering switching overvoltage waveshape. Electr Eng, 102(2): 953–966. https://doi.org/10.1007/s00202-020-00918-7

Beroual A, Dang V-H, Perrier C. 2013. Investigation on creeping discharges propagating over pressboard immersed in mineral and vegetable oils under AC, DC and lightning impulse voltages. IEEE Trans Dielectr Electr Insul, 20(5): 1-6.

Borghei M, Ghassemi M. 2022. Separation and classification of corona discharges under low pressures based on deep learning method. IEEE Trans Dielectr Electr Insul, 29(1): 319–326. https://doi.org/10.1109/TDEI.2022.3146608

Chen Q, Wu Z, Liu F, Yun F, Liu D, Fan J, … Gao C. 2022. The discharge mode of SF6N2Gas mixture in extremely inhomogeneous electric field under power frequency voltage. Conference on Electrical Insulation and Dielectric Phenomena, CEIDP, 13-16 November, pp: 560–563. Institute of Electrical and Electronics Engineers Inc. https://doi.org/10.1109/CEIDP55452.2022.9985344

Chen S, Li K, Wang F, Sun Q, Zhong L. 2019. Effect of humidity and air pressure on the discharge modes transition characteristics of negative DC corona. IET Sci Meas Technol, 13(8): 1212–1218. https://doi.org/10.1049/iet-smt.2019.0032

Dedeoglu S, Merev A. 2023. Realization of the reference composite voltage waveforms for lightning impulse (LI) voltages superimposed over DC and AC signals. Mapan J Metrol Soc India, 38(3): 597–606. https://doi.org/10.1007/s12647-023-00634-0

Dissado LA, Fothergill JC. 1992. Electrical degradation and breakdown in polymers (1st ed.). Institution of Engineering and Technology. London, UK, pp: 54-98.

Dong W, Wang X, Tian B, Liu Y, Jiang Z, Li Z, Zhou W. 2019. Use of grafted voltage stabilizer to enhance dielectric strength of cross-linked polyethylene. Polymers, 11(1): 1-6. https://doi.org/10.3390/POLYM11010176

Dordizadeh P, Adamiak K, Castle GSP. 2017. Experimental study of the characteristics of Trichel pulses in the needle-plane negative corona discharge in atmospheric air. J Electrostat, 88: 49–54. https://doi.org/10.1016/j.elstat.2016.12.013

Fidan M, Ismailoglu H. 2017. Harmonik kaynaklı gerilim bozulmalarının elektriksel kısmi boşalmalar üzerindeki etkilerinin incelenmesi. J Fac Eng Archit Gazi Univ, 32(3): 929–939. https://doi.org/10.17341/gazimmfd.337646

Freitas-Gutierres LF, Maresch K, Morais AM, Nunes MVA, Correa CH, Martins EF, … Oliveira AL. 2024. Framework for decision-making in preventive maintenance: Electric field analysis and partial discharge diagnosis of high-voltage insulators. Electr Power Syst Res, 233: 1-6. https://doi.org/10.1016/j.epsr.2024.110447

Ghassemi M. 2018. PD measurements, failure analysis, and control in high-power IGBT modules. High Volt, 3(3): 170–178. https://doi.org/10.1049/hve.2017.0186

Gong M, Lu M, Liu H, Jiang H, Sun QF, Xie XC. 2020. Transport study of the wormhole effect in three-dimensional topological insulators. Phys Rev B, 102(16): 1-6. https://doi.org/10.1103/PhysRevB.102.165425

Hamidieh M, Ghassemi M. 2024. Conic cross-sectional electrodes and their influence on negative corona discharge and trichel pulse characteristics. IEEE Trans Dielectr Electr Insul, 31(4): 2064–2073. https://doi.org/10.1109/TDEI.2024.3385751

Hu K, Li G, Gu Z, Zhang F, Wei Y, Lei Q. 2023. Analysis of influence factors on ac breakdown characteristics of rod-barrier gap and electric field simulation. J Electr Eng Technol, 18(3): 2189–2197. https://doi.org/10.1007/s42835-022-01259-0

IEC 60060-1:2010. High-voltage test techniques - Part 1: General definitions and test requirements. 2010: 68.

Ispirli MM, Kalenderli Ö, Seifert F, Rock M, Oral B. 2022b. Investigation of impact of DC component on breakdown characteristics for different electric fields under composite AC and DC voltage. High Volt, 7(2): 279–287. https://doi.org/10.1049/hve2.12185

Ispirli MM, Oral B, Kalenderli Ö. 2022a. Electric field analysis of 66 kV and 110 kV SiR insulators under combined AC–DC voltages. Energy Rep, 8: 361–368. https://doi.org/10.1016/j.egyr.2021.11.149

Kadim EJ, Noorden ZA, Adzis Z, Azis N. 2021. Nanoparticles application in high voltage insulation systems. IEEE Trans Dielectr Electr Insul, 28(4): 1380–1399. https://doi.org/10.1109/TDEI.2021.009531

Kavanagh DF, Gyftakis KN, Mcculloch MD. 2020. Thermal degradation phenomena of polymer film on magnet wire for electromagnetic coils. IEEE Trans Ind Appl, 57(1): 458–467. https://doi.org/10.1109/TIA.2020.3040201

Küchler A. 2017. High voltage engineering. Springer eBooks, London, UK, pp: 168. https://doi.org/10.1007/978-3-642-11993-4

Lan G, Bo L, Huanchao C, Jinzhong Li. 2012. Breakdown characteristics of typical model in transformer oil under AC and DC mixed voltage. 2012 October 14–17, 2012 Annual Report Conference on Electrical Insulation and Dielectric Phenomena. IEEE, Ottawa, Canada, pp: 68.

Li Y, Zhang Q, Zhao Y, Wang T, Liu G, Wang K. 2017. The influence of temperature on Partial Discharges and wormhole effect of oil-paper insulation under DC voltage. 2017 June 11–14 IEEE Electrical Insulation Conference (EIC). IEEE, Montreal, Canada.

Li Y, Zhou K, Zhu GY, Zhang QG. 2019. Effect of DC discharges in mineral oil on degradation characteristics of oil-impregnated pressboard. IEEE Trans Dielectr Electr Insul, 26(5): 1701–1708. https://doi.org/10.1109/TDEI.2019.008256

Li Z, He D, Ren F, Li S, Wu H, Sun Y, … Li Q. 2025. Effect of temperature on the internal electric field distribution and discharge mechanism of converter transformer under AC–DC composite voltage. IEEE Trans Dielectr Electr Insul, 32(2): 1084–1093. https://doi.org/10.1109/TDEI.2024.3435815

Liang H, Du B, Li J. 2020. Non-Intrusive measurement of transient electric field distribution under AC and impulse voltages. IEEE Sens J, 20(18): 10898–10902. https://doi.org/10.1109/JSEN.2020.2994246

Lin L, Meng X, Mei H, Wang L. 2024. Influence of AC and DC composite voltage on positive streamer discharge. IEEE Trans Dielectr Electr Insul, 31(2): 779–785. https://doi.org/10.1109/TDEI.2023.3325421

Liu L, Zhang Z, Peng Z, Ouyang J. 2013. Comparison of point-to-plane corona in different gases. J Phys Conf Ser, 418(1): 1-6. Institute of Physics Publishing. https://doi.org/10.1088/1742-6596/418/1/012092

Muppala P, Reddy CC. 2021. Electric field and DC breakdown voltage of multi-layer dielectrics in parallel-plane geometry.

IEEE Trans Dielectr Electr Insul, 28(1): 257–265. https://doi.org/10.1109/TDEI.2020.008830

Negari S, Moghadam DE. 2024. A novel approach towards parametric assessment of reliability and resilience of high voltage mica-based insulation systems by statistical analysis of experimental failure data. High Volt, 9(2): 495–507. https://doi.org/10.1049/hve2.12431

Özkaya M. 2008. Yüksek gerilim tekniği. Birsen Yayınevi, Cilt I, İstanbul, Türkiye, ss: 68.

Park C, Lee K, Kim K, Lim H, Park Y. 2024. Evaluation of Time-Based arc flash detection with non-contact UV sensor. J Electr Eng Technol, 19(3): 1983–1992. https://doi.org/10.1007/s42835-023-01555-3

Qiu Z, Ruan J, Huang D, Pu Z, Shu S. 2015. A prediction method for breakdown voltage of typical air gaps based on electric field features and support vector machine. IEEE Trans Dielectr Electr Insul, 22(4): 2125–2135. https://doi.org/10.1109/TDEI.2015.004887

Reddy BST, Wani SA, Amizhtan SK, Naresh C, Sarathi R. 2023. Understanding the surface discharge activity with nano oil-pressboard insulation under AC and lightning impulse voltages. IEEE Trans Dielectr Electr Insul, 31(2): 889–896. https://doi.org/10.1109/TDEI.2023.3334245

Roggendorf C, Schnettler A. 2012. Accelerated hydrothermal aging of epoxy resin based syntactic foams with polymeric microspheres. IEEE Trans Dielectr Electr Insul, 19(3): 973–980. https://doi.org/10.1109/TDEI.2012.6215102

Rosenberg G, Guo HM, Franz M. 2010. Wormhole effect in a strong topological insulator. Phys Rev B, 82(4): 1-6. https://doi.org/10.1103/PhysRevB.82.041104

Rubinetti D, Iranshahi K, Onwude DI, Nicolaï BM, Xie L, Defraeye T. 2024. Energy-saving discharge needle shape for electrohydrodynamic airflow generation. J Electrostat, 127: 1-6. https://doi.org/10.1016/j.elstat.2023.103876

Saini S, Prasad SD. 2024. Quasi-static ac surface charging of polymeric insulators at low pressure. IEEE Trans Ind Appl, 60(4): 5663–5670. https://doi.org/10.1109/TIA.2024.3397773

Stone G, Boulter EA, Culbert I, Dhirani H. 2014. Electrical insulation for rotating machines. Design, Evaluation, Aging, Testing, and Repair, London, UK, pp:59-67.

Tian H, Liu L, Guo Z, Wang H, Shi R, Peng Z. 2017. Research on electrical field distribution of tri-post insulator and distortion effect by defects. 2017 IEEE Conference on Electrical Insulation and Dielectric Phenomenon (CEIDP). IEEE, 22-25 October, Fort Worth, Texas, USA, pp: 82.

Timoshkin IV, Given MJ, Macgregor SJ, Wilson MP, Lehr JM. 2009. Pre-breakdown currents in insulating liquids stressed with non-uniform DC electric field. 2009 June 12–14 IEEE Pulsed Power Conference, Washington DC, USA, pp: 63.

Tunç E, Fidan M. 2023. Residual voltage tests of 4.5 kV metal oxide surge arrester. 14th International Conference on Electrical and Electronics Engineering, ELECO 2023 - Proceedings. November 30-December 2, Bursa, Türkiye, pp: 18. https://doi.org/10.1109/ELECO60389.2023.10415938

Wu Z, Xu H, Zhou J, Chen Y, Zhang Z, Zhang Q. 2024. Accumulative effect of bipolar oscillation impulse voltage on interturn insulation of transformer winding. IEEE Trans Dielectr Electr Insul, 32(2): 1-6. https://doi.org/10.1109/TDEI.2024.3446768

Yang Y, Gao K, Bi J, Ding L, Yuan S, Wang G. 2022. Influence of micro-water on AC breakdown characteristics of C4F7N/CO2 gas mixture under non-uniform electric field. High Volt, 7(6): 1059–1068. https://doi.org/10.1049/hve2.12215

Zhang B, Ghassemi M, Zhang Y. 2021. Insulation materials and systems for power electronics modules: A review identifying challenges and future research needs. IEEE Trans Dielectr Electr Insul, 28(1): 290–302. https://doi.org/10.1109/TDEI.2020.009041

Zhao L, Su J, Zhang X, Pan Y, Wang L, Fang J, … Cheng J. 2013. An experimental and theoretical investigation into the "wormhole" effect. J Appl Phys, 114(6): 1-6. https://doi.org/10.1063/1.

Zhao L. 2022. A unified formula for five basic forms of discharge in an electric field under short pulses. IEEE Trans Plasma Sci, 50(10): 3400–3411. https://doi.org/10.1109/TPS.2022.3169602

Zhao T, Liu Y, Liu Y, Yang C, Zheng Y, Zhu W, Gu Z. 2024. Bubble motion characteristics in the transformer oil gap at the top of HV Winding. IEEE Transact Dielectrics Electrical Insulat, 1: 3361848. https://doi.org/10.1109/tdei.2024.3361848

Zhao X, Li B, Xiao D, Deng Y. 2017. Breakdown characteristics of CF3I-N2 gas mixtures in a needle-plate geometry. IEEE Transact Dielectrics Electrical Insulation, 24(2): 869–875. https://doi.org/10.1109/tdei.2017.006089

Zheng Y, Zhao T, Tong Y, Chao N. 2021. Simulation of the movement characteristics of micro-bubbles in the oil gap of transformer. 2021 Electrical Insulation Conference, EIC 2021, June 7-28, online, pp: 141–144. https://doi.org/10.1109/EIC49891.2021.9612265

Zhou Y, Huang X, Zhang L, Zhang Y, Zhou Z, Teng C, . . . Huang M. 2020. Space charge characteristics of oil-paper under AC/DC composite voltage. 2022 IEEE Conference on Electrical Insulation and Dielectric Phenomena (CEIDP), September 14-17, Manchester, United Kingdom, pp: 308–311. https://doi.org/10.1109/ceidp49254.2020.9437530